

Experimental study on simplified steel reinforced concrete beam-column joints in construction technology

Masaru Teraoka[†]

Technology Development Division, Fujita Corporation, 2025-1 Ono, Atsugi-shi, Kanagawa, Japan

Koji Morita[‡]

*Department of Design and Architecture, Faculty of Engineering, Chiba University
1-33 Yayoi-cho, Chiba-shi, Chiba, Japan*

Satoshi Sasaki^{‡†} and Daisuke Katsura^{‡†}

Technology Development Division, Fujita Corporation, 2025-1 Ono, Atsugi-shi, Kanagawa, Japan

Abstract. The purpose of this paper is to propose a new type of steel reinforced concrete (SRC) beam-column joints and to examine the structural performance of the proposed joints, which simplify the construction procedure of steel fabrication, welding works, concrete casting and joint strengthening. In the proposed beam-column joints, the steel element of columns forms continuously built-in crossing of H-sections ($\text{H} \perp \text{H}$), with adjacent flanges of column being connected by horizontal stiffeners in a joint at the level of the beam flanges. In addition, simplified lateral reinforcement ($\text{S} \times \text{S}$) is adopted in a joint to confine the longitudinal reinforcing bars in columns. Experimental and analytical studies have been carried out to estimate the structural performance of the proposed joints. Twelve cruciform specimens and seven SRC beam-column subassembly specimens were prepared and tested. The following can be concluded from this study: (1) SRC subassemblages with the proposed beam-column joints show adequate seismic performances which are superior to the demand of the current code; (2) The yield and ultimate strength capacities of the beam-to-column connections can be estimated by analysis based on the yield line theory; (3) The skeleton curves and the ultimate shear capacities of the beam-column joint panel are predicted with a fair degree of accuracy by considering a simple stress transfer mechanism.

Key words: new type of SRC beam-column joint; simplifying construction procedure; structural performance; limit analysis; yield line theory.

1. Introduction

A steel reinforced concrete (SRC) structure is excellent in performance for earthquake and fire resistance. As Japan is located in a strong seismic region, SRC structure is adopted for a lot of middle-rise and high-rise buildings. But SRC structure is complicated in construction technology, compared

[†]General Research Manager

[‡]Professor

^{‡†}Research Engineer

with reinforced concrete or steel structure. Therefore, development of SRC structure aimed at simplification in construction technology is strongly desired (AIJ 1987).

Considering above mentioned background, the purpose of this paper is to propose a new type of SRC beam-column joint and to examine the structural performance of the proposed joints, which simplify the construction procedure of steel fabrication, welding works, concrete casting and joint strengthening. Two kinds of tests are planned. One is experiment for cruciform specimens of beam-to-column connections in the tensile side of the a joint, and the other is that of beam-column subassembly. In the former experiment, the strength capacity of beam-to-column connections is analyzed based on the yield line theory. The beam-column subassembly experiment indicates whether the evaluation method for strength capacity in cruciform specimen is applicable to beam-to-column connections in frame and structural behavior of beam and joint panel. A part of this research is already published (Teraoka *et al.* 1992, 2000).

2. Proposed new type of SRC beam-column joints

The geometrical configuration of the proposed new type of SRC beam-column joint is shown in Fig. 1. The new type joint is proposed in order to simplify the construction procedure of steel fabrication, welding works, concrete casting and joint strengthening. In the joint, the steel element of column forms continuously built-in crossing of H-sections (\oplus), and adjacent flanges of column are connected by horizontal stiffeners in a joint at connecting levels of beam flanges. Also simplified lateral reinforcement (\otimes) is adopted in a joint to confine the longitudinal reinforcement bars in columns (Taniguchi *et al.* 1988, Matsui *et al.* 1989).

3. Experiments on cruciform specimens

3.1. Outline of experiments

Twelve specimens were prepared and tested. The configuration and details are shown in Fig. 2 and Table 1 respectively. The main parameters for the tests are (a) the thickness of the column web (c, t_w), (b)

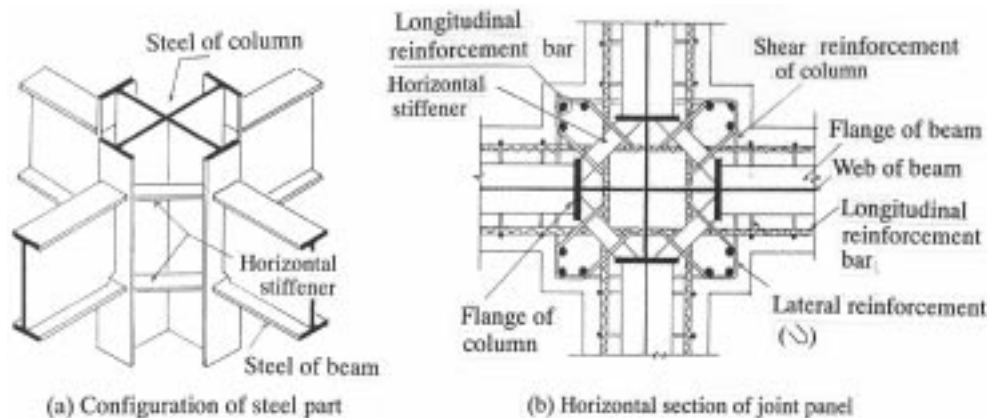


Fig. 1 Proposed new type of SRC beam-column joints

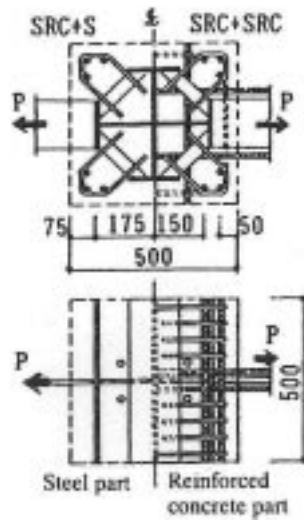


Fig. 2 Details of cruciform specimens

Table 1 Dimensions and test parameters of cruciform specimens

Series	Specimen	Type of structural members		Column	Joint	Beam	
		Column	Beam	Thickness of webs and flanges $t_w \times t_f$	Section of stiffeners $s_t \times_s W$	Lateral reinforcement	Flange dimension
I	CNO.1	SRC	S	9×12	12×40	R	16×150
	CNO.2	SRC	SRC	9×12	12×40	R	16×150
	CNO.3	SRC	SRC	9×12	12×40	N1	16×150
	CNO.4	SRC	S	9×12	19×40	R	16×150
	CNO.5	SRC	SRC	9×12	19×40	R	16×150
	CNO.6	SRC	SRC	9×12	12×40	R	16×150
	CNO.7	SRC	SRC	6×12	12×40	R	16×150
	CNO.8	SRC	S	6×12	25×45	R	16×150
II	CNO.9	SRC	S	9×12	9×30	R	16×130
	CNO.10	SRC	SRC	9×12	9×30	R	16×130
	CNO.11	SRC	SRC	9×12	9×30	N2	16×130
	CNO.12	SRC	SRC	9×12	16×40	R	12×130

[Notes]

Column: Section $b \times_c D = 500 \times 500$ mm, Steel section \mp -350×150× t_w × t_f

Longitudinal reinforcement: 12-D19

Joint: Lateral reinforcement R: \boxtimes -D10@50, N1: \square -D10@50, N2: \square -D10@62.5

Beam: Longitudinal reinforcement of SRC type: 4-D16

the thickness of the column flange (t_f), (c) the stiffener's dimension ($s_t \times_s W$), (d) the type of joint reinforcing (N: normal type (\square), R: simplified type (\boxtimes)), (e) the beam flange dimension ($b_{t_f} \times_b b_f$) as for two structural form (i) SRC column-S beam (4 specimens), (ii) SRC column-SRC beam (8 specimens). Mechanical properties of materials are shown in Table 2.

The specimens were tested by monotonic tensile loading. Local deformation of beam-to-column

Table 2 Mechanical properties of materials
(a) Steel

Series	Plate	Measured thickness	Yield point	Tensile strength	Series	Bar	Yield point	Tensile strength
		t	σ_y	σ_u			σ_y	σ_u
I	PL-6	5.55	381	558	I	7 ϕ	300	457
	PL-9	8.78	359	544		D10	353	525
	PL-12	11.42	353	545		D16	403	563
	PL-16	15.38	367	551		D19	442	621
	PL-19	18.43	346	544		D22	441	634
	PL-25	24.13	351	551		7 ϕ	300	457
II	PL-6	5.66	403	548	II	D10	354	492
	PL-9	8.5	367	550		D16	403	563
	PL-12	11.5	377	542		D19	472	649
	PL-16	15.85	333	517				

Units: t (mm), σ (N/mm²)

(b) Concrete

Series	Used part ^{*1}	Compressive strength	Strain at compressive strength	Tensile splitting strength
		σ_B	ϵ_B	σ_{st}
I	C1	36	2243	2.79
	C2	40	2159	3.99
	C3	39	2137	3.61
	C4	38	2392	3.54
II	C5	47	2582	2.91
	C6	39	2540	2.35

Units: σ (N/mm²), ϵ (10⁻⁶)

*1: C1: Cruciform specimens for series I

C2: Joint panels, beams and lower columns for series I of subassemblage specimens

C3: Upper columns for SNO.1 and SNO.3

C4: Upper columns for SNO.2 and SNO.4

C5: Cruciform specimens for series II, joint panels, beams and lower columns for series II of subassemblage specimens

C6: Upper columns for series II of subassemblage specimens

connections (Δ , see Fig. 3) and strain in the vicinity of beam-to-column connections were measured.

3.2. Outline of test results

Load (P)-local deformation (Δ) relationships ($\Delta \leq 3$ mm) are shown in Fig. 4. Yield tensile strength (${}_eP_{PJ}$), maximum tensile strength capacity (${}_eP_m$) of beam-to-column connections and failure mode are shown in Table 3. ${}_eP_{PJ}$ is identified by the general yield point method considering the strain of each parts of the connections. Two failure modes were found: one is failure at beam-to-column connections (JF) and the other is failure at beam end parts (BF) (see Fig. 3). Strength capacities of beam-to-column connections increase with the increase of $c_t \times w$, $c_t f$ and $s_t \times s W$ and the amount of longitudinal reinforcement bars in beams. On the other hand, the influence due to the difference of lateral reinforcement types was not found.

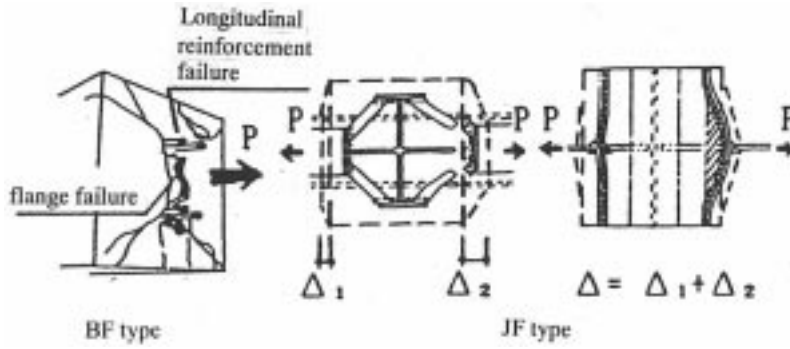
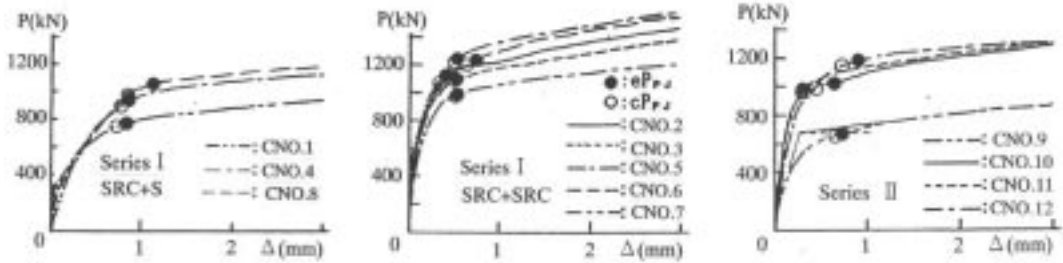


Fig. 3 Failure mode for cruciform specimens


 Fig. 4 Experimental P - Δ relationships of cruciform specimens

3.3. Discussion on strength capacities of cruciform specimens

The yield strength capacities of beam-to-column connection were estimated by using “the yield line theory” with the assumption that the yield mechanism is modeled at the connections as shown in Fig. 5 and the allowable stress intensity of cone failure in covering concrete is assumed as $0.19\sqrt{\sigma_B}N/mm^2$. (Morita *et al.* 1990, Teraoka *et al.* 1992). Yield strength capacities of cruciform specimens are expressed as Eq. (1).

$${}_cP_{PJ} = 4{}_fM_P/X + {}_wT_y(X+t) + \sqrt{2}{}_sN_y + {}_bN_y + \{2(2X+t + {}_cb_f) {}_cd + \pi \cdot {}_cd^2\} \cdot 0.19\sqrt{\sigma_B} \quad (1)$$

in which

$${}_fM_P = {}_c\sigma_y \cdot {}_ct_f^2 \cdot {}_cb_f/4,$$

$${}_wT_y = {}_ct_w \cdot {}_w\sigma_y,$$

$${}_sN_y = {}_st \cdot {}_sW \cdot {}_s\sigma_y,$$

$${}_bN_y = {}_Ar \cdot {}_r\sigma_y,$$

$$X = \sqrt{4{}_fM_P / ({}_wT_y + 4{}_cd \times 0.19\sqrt{\sigma_B})},$$

where ${}_c\sigma_y$, ${}_w\sigma_y$, ${}_s\sigma_y$ are respectively yield strength of column flange, column web, stiffener and ${}_Ar$, ${}_r\sigma_y$ are the total area and yield strength of the longitudinal reinforcement bars in the beam respectively. Other notations can be seen in Fig. 5. In the case of the steel beam, the effect of

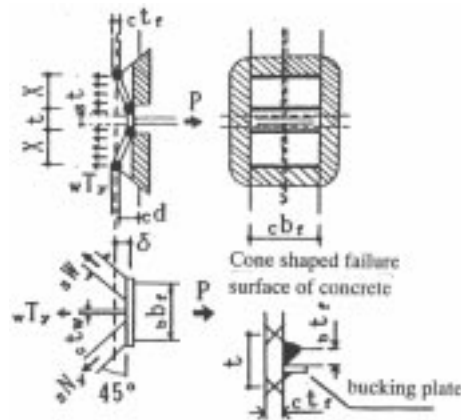


Fig. 5 Assumed yield line mechanism for cruciform specimen

cover concrete should be neglected.

The comparison between experimental values (eP_{PJ}) and estimated values (cP_{PJ}) of strength capacities is shown in Table 3 and Fig. 4. The ratio of eP_{PJ}/cP_{PJ} ranges from 1.00 to 1.08 (the average value is 1.03),

Table 3 Test results in comparison with estimated strength capacities

Series	Specimens	At yield strengths of beam-to-column connections				At maximum load				Failure mode*4	
		Yield strength		Deformation	Maximum strength			Deformation			
		Exp. eP_{PJ}	Est. cP_{PJ} *1	$\frac{eP_{PJ}}{cP_{PJ}}$	Δ_{PJ}	Exp. eP_m	Est. cP_{mj} *2	Ext. cP_{mj} *3	$\frac{eP_m}{cP_m}$		Δ_m
I	CNO.1	755	738	1.02	0.86	1156	1141	1271	1.01	12.3	JF
	CNO.2	1108	1060	1.05	0.40	1687	1589	1719	1.06	8.6	JF
	CNO.3	1079	1060	1.02	0.57	1707	1589	1719	1.07	12.8	JF
	CNO.4	922	872	1.06	0.84	1264	1302	1271	0.99	8.0	BF
	CNO.5	1226	1192	1.03	0.50	1755	1803	1719	1.02	9.5	BF
	CNO.6	1216	1189	1.02	0.74	1753	1778	1719	1.02	4.6	BF
	CNO.7	971	961	1.01	0.51	1489	1428	1719	1.04	13.4	JF
	CNO.8	1030	951	1.08	1.11	1266	1475	1271	1.00	5.3	BF
II	CNO.9	657	656	1.00	0.73	970	986	1058	0.98	7.4	JF
	CNO.10	1010	975	1.04	0.62	1481	1432	1511	1.03	8.4	JF
	CNO.11	981	977	1.00	0.26	1482	1434	1510	1.03	8.8	JF
	CNO.12	1167	1130	1.03	0.90	1313	1679	1254	1.05	4.1	BF

Notes, units P (KN), Δ (mm).

*1: cP_{PJ} : Estimated values by Eq. (1)

*2: cP_{mj} : Maximum strength capacities is calculated by using Eq. (1), applying σ_u and $0.32\sqrt{\sigma_B}$ instead of σ_y and $0.19\sqrt{\sigma_B}$, respectively.

*3: cP_{mj} : Ultimate tensile strength of flange and longitudinal reinforcement bars in beam

*4: BF is tearing failure of beam flange and longitudinal reinforcement, JF is failure of beam-to-column connection.

Table 4 Dimensions and test parameters for subassemblage specimens

Series	Specimen	Column	Joint	Beam		Corresponded cruciform specimen	
		Thickness of webs and flanges	Section of stiffeners	Lateral reinforcement	Flange dimension		Longitudinal reinforcement
		$t_w \times c t_f$	$s t \times_s W$		$b t_f \times_b b_f$		
I	SNO.1	9×12	12×40	R	16×150	B1	CNO.2
	SNO.2	9×12	19×40	R	16×150	B1	CNO.5
	SNO.3	6×12	12×40	R	16×150	B1	CNO.7
	SNO.4	6×12	25×45	R	16×150	B2	CNO.8
II	SNO.5	9×12	9×30	R	16×130	B3	CNO.10
	SNO.6	9×12	9×30	N	16×130	B3	CNO.11
	SNO.7	9×12	16×40	R	12×130	B3	CNO.12

[Notes]

Column: Section $b \times_c D = 500 \times 500$ mm, Steel section \boxplus -350×150× $c t_w \times c t_f$

Longitudinal reinforcement: 12-D19, Shear reinforcement: \square -D10@50

Joint: Lateral reinforcement R: \boxtimes -D10@50, N: \square -D10@62.5

Beam: Section $b b \times_c D = 300 \times 500$ mm, Steel section H-350× $b b_f \times 6 \times_b t_f$

Reinforcement: Longitudinal (Top/Bottom), Shear reinforcement

B1:4-D16, \square -7 ϕ @100

B2:4-D22, \square -7 ϕ @70

B3:2-D16, \square 7 ϕ @100

amount of longitudinal reinforcing bars in beams.

The mechanical properties of materials are shown in Table 2.

The specimens were tested by incremental lateral loading reversals at both ends of beams, while constant axial load was applied to the columns.

4.2. Outline of test results

The outline of test results is shown in Table 5. The yield strength capacities of beam-to-column connections ($e Q_{Pj}$) were evaluated by the general yield point method from synthetic curves (Kato 1982) of beam load (Q_b)-local deformation of beam-to-column connections (Δ_n) relationships (see Fig. 12). Structural behavior of the beams shows very complicated manners due to the influence of a reciprocal reaction with beam-column interactions.

Fig. 7 shows hysteresis curves between Q_b and inter story drift angle (R_T). The maximum strength capacities were recorded at the angles of $R_T = 30 \sim 40 \times 10^{-3}$ rad. (cumulative value; $R_{Tma} = 18.5 \sim 24.9 \times 10^{-3}$ rad.). From the figure, it is clear that the hysteresis curves indicate restoring force characteristics with relatively high toughness.

In Japan, the ordinary moment frame structures designed based on “Ultimate Strength and Deformation Capacity of Building in Seismic Design (1990)” figures that the ductility factor of each inter story of the building is more than 4, according to equal maximum potential response (AIJ 1990). That is equivalent to the inter story drift angle being more than 20×10^{-3} rad. In the customary design of high-rise frames, the inter story drift angles are usually permitted up to 10×10^{-3} rad. On the other hand, in the United States, by the criteria of FEMA-350 (FEMA 2000), the inter story drift angles of ordinary moment frame is limited to 20×10^{-3} rad. Seismic performance obtained from this tests was larger than

Table 5 Test results in comparison with estimated strength capacities for subassembly specimens

Specimen	At yield strength of beams								Yield strength of beam-to-column connections		At maximum load						Yielding process and failure mode ^{*4}		
	Yield strength				Deformation						Maximum strength		Beam deformation		Inter story drift				
	Exp. cQ_{bp}	Est. ^{*1} cQ_{bp}	$\frac{eQ_{bp}}{cQ_{bp}}$	R_{bpa}	R_{bpa}'	cR_{bp}	$\frac{R_{bpa}'}{cR_{bp}}$	Exp. eQ_{pj}	Est. ^{*2} cQ_{pj}	$\frac{eQ_{pj}}{cQ_{pj}}$	Exp. eQ_{bm}	Est. ^{*3} cQ_{bm}	$\frac{eQ_{bm}}{cQ_{bm}}$	R_{bma}	R'_{bma}	R_{Tm}		R_{Tma}	
SNO. 1	+	338	332	1.02	9.5	8.2	5.6	1.46	309	302	1.02	383	363	1.06	17.6	11.0	30.0	21.8	JY → BY, PY → PF
	-	314		0.94	8.8	6.5		1.16	294		0.97	364	(380)*	1.00	14.6	7.6	30.0	20.0	
SNO. 2	+	333	332	1.00	8.5	7.9	5.6	1.40	-	362	-	390	404	0.97	16.6	12.5	30.0	21.3	BY, PY → JY → PF
	-	324		0.97	8.5	7.8		1.39	-		-	380	(380)	0.93	16.3	13.0	30.0	22.7	
SNO. 3	+	333	332	1.00	11.7	9.8	5.6	1.74	265	231	1.14	352	338	1.04	15.0	11.3	30.0	20.4	JY → PY → BY → PF
	-	329		0.99	11.0	6.5		1.16	255		1.10	335	(349)*	0.99	12.2	6.4	30.0	18.5	
SNO. 4	+	436	409	1.07	12.0	9.2	6.0	1.55	-	402	-	447	410	1.07	14.5	10.8	30.0	21.4	PY → JY → BY → PF
	-	417		1.02	11.5	8.5		1.43	-		-	422	(349)*	1.05	12.4	9.5	30.0	20.3	
SNO. 5	+	275	255	1.08	8.3	6.7	4.2	1.59	245	228	1.07	351	330	1.06	21.9	13.7	40.0	24.0	JY → BY → PY → JF
	-	265		1.04	8.7	6.2		1.48	235		1.03	343		1.04	22.3	13.9	30.0	24.9	
SNO. 6	+	275	255	1.08	8.2	6.9	4.2	1.65	255	228	1.12	347	330	1.05	20.3	11.5	40.0	22.8	JY → BY → PY → JF
	-	275		1.08	9.2	6.8		1.63	245		1.07	343		1.04	20.5	13.1	30.0	22.7	
SNO. 7	+	240	228	1.05	7.0	7.1	4.1	1.73	309	298	1.04	321	303	1.06	21.4	20.5	30.0	22.0	BY → JY → BF
	-	216		0.94	6.2	6.4		1.56	279		0.94	330		1.09	23.2	22.1	40.0	24.5	

Notes, units Q (KN), R (10^{-3} rad.)

*1 cQ_{bp} : Calculated value by estimation method presented at 4.3.1

*2 cQ_{pj} : Calculated value by Eqs. (2), (3), (4)

*3 cQ_{bm} : For SNo. 1~ SNo. 4, ultimate shear strength(cQ_{PUB}) of joint panel calculated by Eq. (5), and () * is calculated value ($_{SR}Q_{Pu}$) based on SRC-standard (AIJ 1987).

For SNo. 5 and SNo. 6 ultimate strength (cQ_{mj}) of beam to column connection calculated by Eq. (4), applying σ_u instead of σ_y .

For SNo. 7, ultimate bending capacities (cQ_{bm}) calculated by the method presented at 4.3.1.

*4: Failure mode: BY, JY and PY mean yielding of beam, joint, joint and panel.

BF is flexural compressive failure of concrete at beam end.

PF is shear failure of Joint panel.

JF is failure of beam-to-column connection.

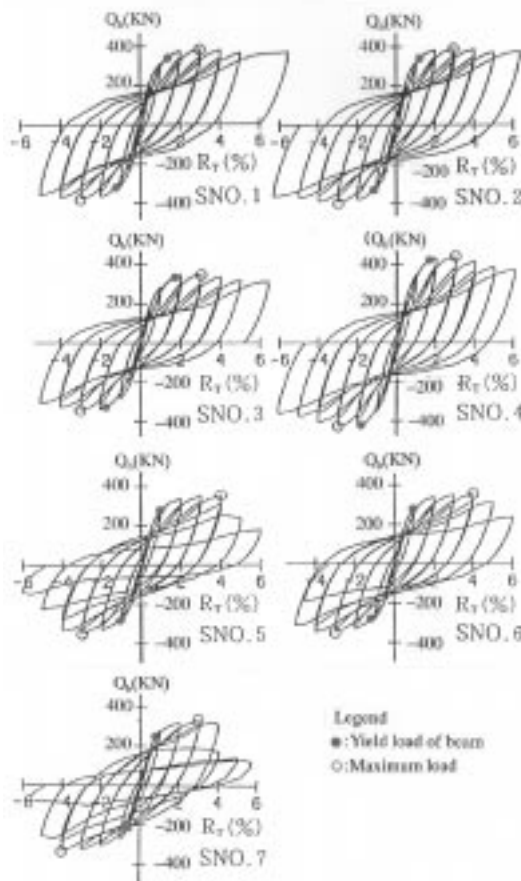


Fig. 7 Beam load(Q_b)-inter story drift angles (R_r) hysteresis loops

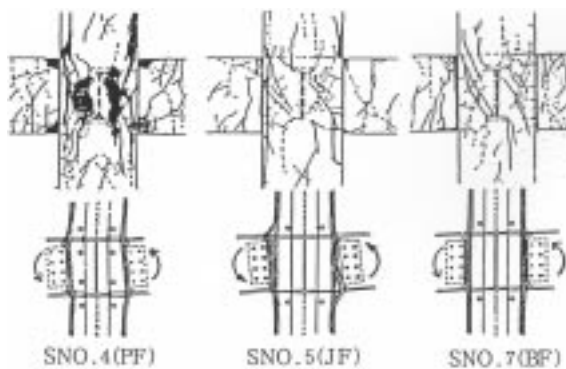


Fig. 8 Typical failure patterns in concrete and steel

the demands of those criteria, which indicate that the SRC structure with the proposed beam-column joints have sufficient seismic performance.

Specimen SNO. 1~SMO. 4 were broken by shearing failure at the joint panels (PF). Specimen SNO.

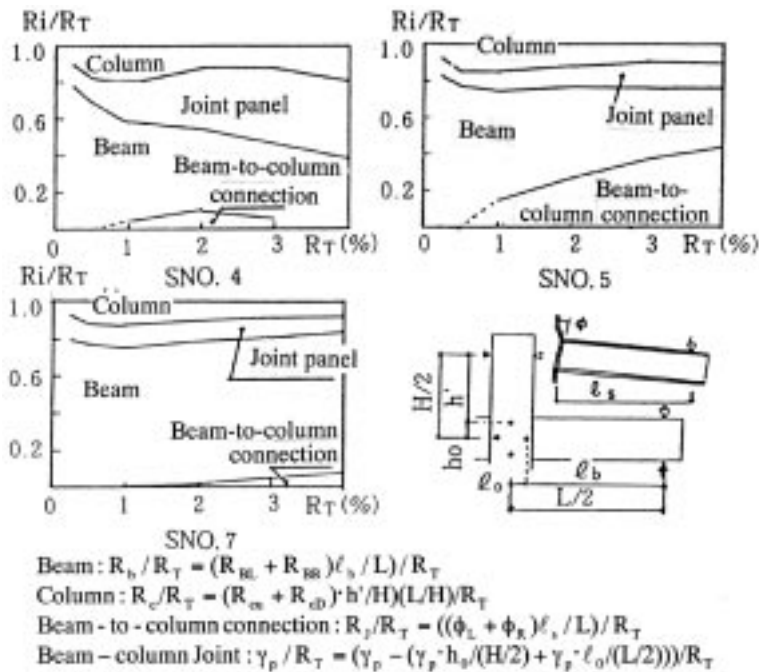


Fig. 9 Ratio of each structural part deformation to inter story drift angle

5~SNO. 6, were broken by failure at beam-to-column connections (JF) Specimen SNO. 7~SNO. 8 were broken by failure caused by bending moments in beam-end parts (BF). Fig. 8 illustrates typical patterns of each failure mode in concrete and steel beams at joints.

Fig. 9 shows the ratio of the inter story drift angle (R_i) of each structural part to total inter story drift angle R_T . The figures indicate that the drift angle of joint panels is dominant in failure mode PF, the local drift angle at beam-to-column connections in mode JF, and the beam drift angle in mode BF.

Regarding the influence of structural performances due to the difference of experimental parameters, the strength capacities at beam-column joint panels and the beam-to-column connections increase with the increase of $c t_w$, $s t_w \times_s W$ and the amount of longitudinal reinforcement bars in beams. On the other hand, the influence due to the difference of lateral reinforcement bar types was not found. This tendency is same with the cruciform test.

4.3. Discussion

4.3.1. Mechanical behavior of beams

(1) Bending strength capacity

The bending strength capacities at beam ends were calculated based on Navier's assumption by adopting the stress-strain relationship of concrete as e -Function (Umemura 1951) and that of steel as bi-linear relationship (in this relationship, $Est = 0.15 E$, where E is Young's modulus of steel and Est is the modulus of steel after yield strength). Regarding yield bending strength capacities of beam ends, the calculated values $c Q_{bP}$ ($c Q_{bP} = {}_b M_P / l_b$, where ${}_b M_P$ shows the bending moment at the yield stage in the main tension reinforcement bars and the flanges, l_b shows the distance between loading points and

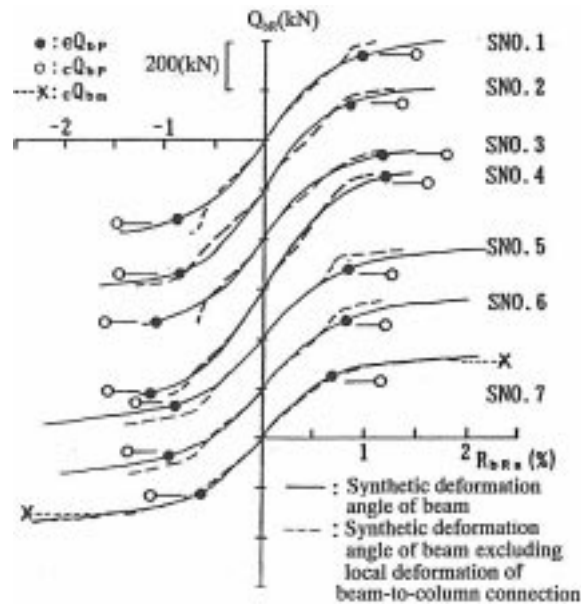


Fig. 10 Synthetic curves of Q_b - R_{ba} (R_{ba}') relationships

longitudinal reinforcement bars of columns) and the measured values eQ_{bP} are shown in Table 5 and Fig. 10 respectively. In Fig. 10, the relationship between Q_b and R_{ba} (R_{ba}') is also shown. The ratios of eQ_{bP}/cQ_{bP} ranged from 0.94 to 1.08 (the average value is 1.02), and the measured values are in agreement with the calculated values.

Regarding the maximum strength capacity of SNO. 7 whose failure mode is BF, the calculated value (cQ_{bm}) is also in agreement with the measured value as shown in Table 5.

(2) Deformation

Fig. 10 shows the comparison between the skeleton curve of beams calculated from bending deformation (obtained from the integration of curvature distribution in the beam) by adding elastic shear deformation and the measured values of Q_b - R_{ba}' relationship. From the figure, it is observed that the calculated values have relatively high agreement with the tendencies of measured values. Nevertheless, for the initial stiffness and the deformation at yield stage, the calculated values are smaller than the measured values. For the deformation at the stage of yield bending resistance, the calculated values are smaller than measured values as shown in Table 5, because the ratio between the measured values and calculated values (R_{bPa}'/cR_{bP}) ranges from 1.16 to 1.74. The difference is probably due to the fact that the residual stress of steel, shrinkage stress of concrete and bond deterioration of longitudinal reinforcement bars are not considered in the calculation, and that the beam-column joints have a significant affect on the behavior of the beams. Further investigation is required to improve the level of agreement.

Regarding the angle of rotation at the maximum capacities, the values of specimen which have a failure mode of PF are relatively small because R_{bma} ranges from 12.2 to 23.2×10^{-3} rad. and R_{bma}' ranges from 6.4 to 22.1×10^{-3} rad. as shown in Table 5 and Fig. 10. The values of specimens which have a failure mode of JF are almost similar to those whose failure mode is BF in R_{bma} , on the other hand the values of R_{bma}' of JF type are smaller than those of BF type. In the specimen SNO.7 which has failure

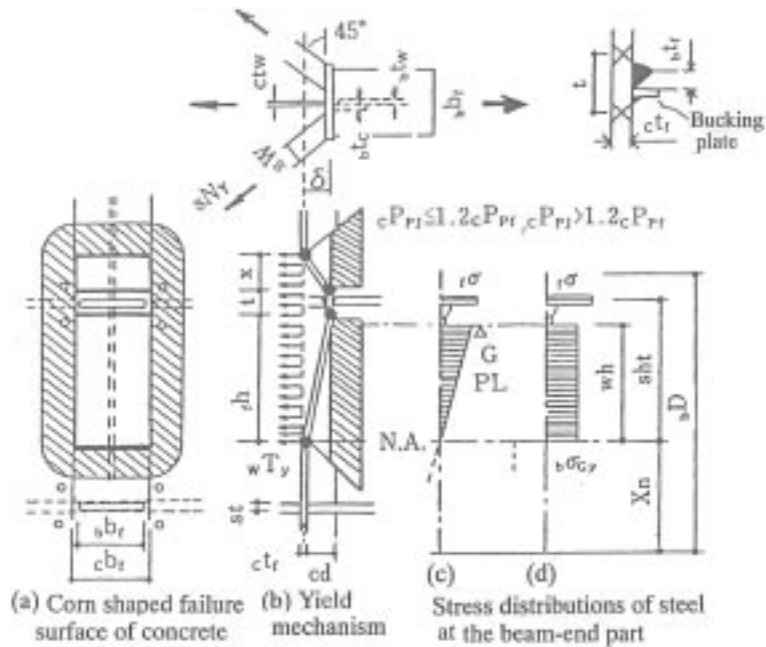


Fig. 11 Assumed yield line mechanism for beam-to-column connection of subassemblage specimen

type BF, the values of R_{bma} are almost similar to those of R_{bma}' , which indicates the local deformation at the column-beam joints can be neglected.

4.3.2. Strength capacities of the beam-to-column connections

The yield strength capacities of beam-to-column connections were estimated by using “the yield line theory” with the assumption that the yield mechanism is modeled at the connections as shown in Fig. 11(a), (b) and the stress of the beam end is distributed as shown in Fig. 11(c), (d) (Morita *et al.* 1990, Teraoka *et al.* 1992). The detailed estimation procedure is shown below:

(i) At first, the flange tensile stress of beams (f_s) by the arbitrary bending moments (bM), and the distance (X_n) between the extreme compression fiber and the neutral axis are calculated from bending moment analysis at the beam-end section.

(ii) Next, X_n is calculated based on the assumption that the ratio between full yield bending moment capacities of the beam (bM_p) and the bending moment of the beam at the beam-end (M_j) can be approximated from the ratio between yield strength capacities of the tensile part of the beam ($cP_{Pf} = b t_f \cdot b b_f \cdot f_s \sigma_y + A_r \cdot r_s \sigma_y$, where $f_s \sigma_y$ is the yield strength of beam flange, A_r and $r_s \sigma_y$ are total area and yield strength of tensile longitudinal reinforcement in beam) and the tensile yield strength capacities at the beam-to-column connection for cruciform model respectively (cP_{PJ} , see Eq. (1)). Namely, by assuming next relationship $cP_{PJ}/cP_{Pf} \doteq M_j/bM_p$, X_n is calculated from the relationship between $M_j \doteq bM_p \cdot cP_{PJ}/cP_{Pf}$ and X_n previously calculated in (i).

(iii) Finally, by using X_n obtained from (ii), corresponding f_s is defined by considering following conditions.

(1) $cP_{PJ} < cP_{Pf}$ (The case where the connection yields prior to the beam-end)

In this case, the stress distribution of the beam-end is assumed as shown in Fig. 11(c), and the

allowable stress intensity of the cone failure surface in covering concrete is assumed as $0.19\sqrt{\sigma_B}$ (Morita *et al.* 1990).

$${}_f\sigma = (B \cdot {}_wT_y + 2C \cdot {}_fM_p + \sqrt{2}{}_sN_y + D)/A \quad (2)$$

in which

$$A = {}_bt_f \cdot {}_bb_f + {}_bt_G \cdot {}_wh^3 / (3{}_sh_t^2),$$

$$B = X/2 + t + ({}_sh_t - t)/2,$$

$$C = 1/X + 1/{}_fh,$$

$$D = \{2(X + t/2 + {}_sh_t + {}_cb_f) \cdot {}_cd + \pi \cdot {}_cd^2\} \times 0.19\sqrt{\sigma_B},$$

$$X = \sqrt{4{}_fM_p / ({}_wT_y + 0.77{}_cd\sqrt{\sigma_B})},$$

where ${}_wT_y$, ${}_fM_p$, ${}_sN_y$ are seen in Eq. (1), other notations are seen in Fig. 11.

(2) ${}_cP_{Pf} < {}_cP_{PJ} \leq 1.2 {}_cP_{Pf}$ (The case where the beam-end yields prior to the connection)

In this case, the stress distribution of the beam-end is assumed as shown in Fig. 11(c). Also, as it is predicted that the beam-end yields prior to the connection and the cyclic loading are applied, the covering concrete is assumed to have no resistance effect.

$${}_f\sigma = (B \cdot {}_wT_y + 2C \cdot {}_fM_p + \sqrt{2}{}_sN_y)/A \quad (3)$$

in which A , B , ${}_wT_y$, C , ${}_fM_p$ and ${}_sN_y$ are seen in Eqs. (1) and (2), provided that $X = \sqrt{4{}_fM_p / {}_wT_y}$.

(3) $1.2 {}_cP_{Pf} < {}_cP_{PJ}$ (The case where the beam-end yields considerably prior to the connection)

In this case, the stress distribution of the beam-end is assumed as shown in Fig. 11(d). Also the covering concrete is assumed to have no resistance effect as described in (2).

$${}_f\sigma = (B \cdot {}_wT_y + 2C \cdot {}_fM_p + \sqrt{2}{}_sN_y - G) / ({}_bt_f \cdot {}_bb_f) \quad (4)$$

in which B , ${}_wT_y$, C , ${}_fM_p$, ${}_sN_y$ and X are seen in Eq. (3) and $G = {}_b\sigma_{Gy} \cdot {}_bt_G \cdot {}_wh^2 / (2{}_sh_t)$, where ${}_b\sigma_{Gy}$ is the yield strength of the gusset plate in the connections.

By using ${}_f\sigma$ obtained from procedure mentioned above, the corresponding X_n is defined from the previously calculated results shown in (i). The procedure of bending stress analysis at the beam-end is the same method presented in 4.3.1 (Umemura 1951). Then the convergence calculations are repeated until the constant X_n coincides with the assumed value in (iii). ${}_bM$ calculated in (1) using X_n is the yield bending moment of the beam to column connection (${}_pM_J$). Regarding the yield strength capacities, the comparison between the measured values (${}_eQ_{PJ}$) and the estimated values (${}_cQ_{PJ} = {}_pM_J / l_s$, where l_s shows the distance between the loading point of the beam and the column flange) are shown in Table 5, Fig. 12 (which shows synthetic curves of $Q_b - \Delta_a$ relationships) respectively. The ratio of ${}_eQ_{PJ} / {}_cQ_{PJ}$ ranges from 0.94 to 1.14 (the average value is 1.05), and they are in fairly high agreement.

The maximum resistance capacities of both SNO.5 and SON.6, which have JF-type failure modes, are estimated by using the same estimation procedure of substituting σ_y with σ_u . As shown in Table 5, Fig. 12, the measured values (${}_eQ_{bm}$) and the estimated values (${}_cQ_{mj}$) have high agreement.

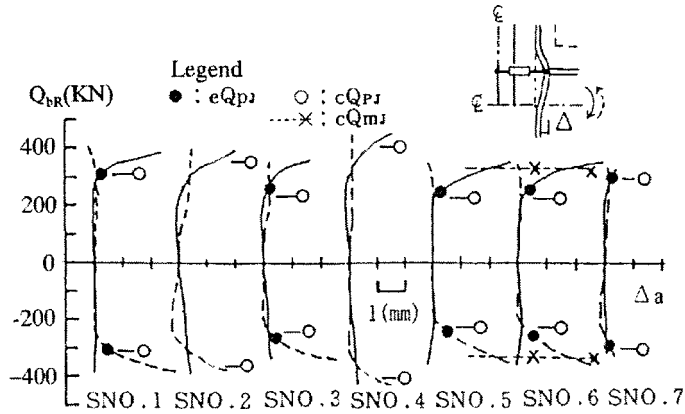


Fig. 12 Synthetic curve of $Q_{bR}-\Delta_a$ relationships

4.3.3. Mechanical behavior of the joint panel

(1) Ultimate shear strength capacities

Regarding specimen SNO.1~SNO.4 with PF-type failure modes, the ultimate strength capacities ($_{SR}Q_{PU}$), obtained by adding the resistance capacities of orthogonal flange ($1.2 \times 4_{fOF} M_p / b h_w$, where $_{fOF} M_p$ is seen in Eq. (5)) to the ultimate resistance capacities based on SRC-standard (AIJ 1987), are in high agreement with the measured values ($_{e}Q_{bm}$) in SNO.1~SNO.3. But, in specimen SNO.4 whose stiffer resistance capacity is higher than that of specimen SNO.3, the measured value ($_{e}Q_{bm}$) is relatively higher than the calculated value ($_{SR}Q_{pu}$).

In order to take the effect of stiffer resistance capacity into account, the ultimate resistance capacity was estimated by using the assumed stress transfer mechanism as shown in Fig. 13. Namely, the resistance capacity of concrete at joint sections was calculated in the core part, the core side part and covering part respectively. In the core part and the core side part, the compression strut mechanism was assumed. Especially in the core side part, the resistance capacity was evaluated by adopting lower values among compression strut resistance capacity and stiffer resistance capacity. In the covering

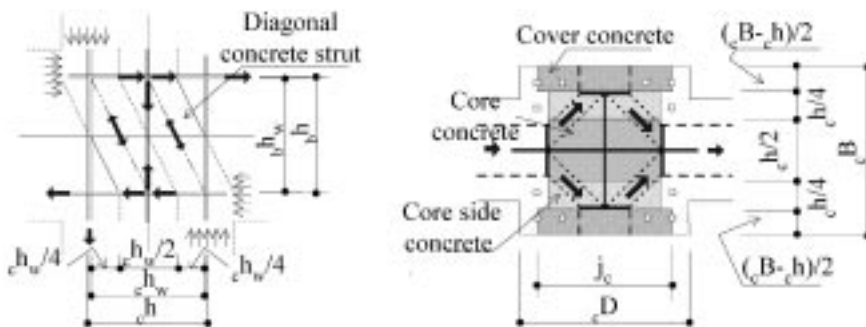


Fig. 13 Assumed stress transfer mechanism for the joint panel of subassembly specimen

part, the allowable shear strength was assumed to be $0.57\sqrt{\sigma_B}$ (AIJ 1987) because the restraint effect was not expected. Consequently, the equation for ultimate resistance capacity was obtained from Eq. (5). In the equation, the concrete resistance capacity is added to the resistance capacities of column web and orthogonal column flange.

$$Q_{pu} = c_h \cdot T_y / \sqrt{3} + 4_{fOF} M_p / b h_w + Q_{cp} + MIN \cdot (Q_{cp}, 2\sqrt{2_s} N_y) + 0.57\sqrt{\sigma_B} (cD - c h) \cdot c_j \quad (5)$$

in which

$$_{fOF} M_p = c_{\sigma_y} \cdot c_{t_f} \cdot c_b^2 / 4,$$

$$Q_{cp} = ({}_b h \cdot c_{h^2} \cdot c_{h_w} \cdot \sigma_B) / (4{}_b h^2 + c_{h^2}),$$

where other notations are seen in Fig. 13.

In Table 5, the comparison between estimated values (${}_c Q_{PUb} = {}_c Q_{PU} / (2l_b / b h - L/H)$), obtained by substituting the estimated values in Eq. (5) with beam loads, and the measured values are shown. The ratio of ${}_b Q_m / {}_c Q_{PUb}$ ranges from 0.93 to 1.07 (the average value is 1.01), and the estimated values are in high agreement with the measured values. Also, the difference of stiffener resistance capacities can be well explained.

(2) Skeleton curves of shear force (Q_p)-shear distortion (γ_p) relationships in joint panels

The skeleton curve of the joint panel was predicted by the summation of the values in each part after evaluating the $Q_p - \gamma_p$ relationship of each part respectively as shown below;

Web of column $Q_{Pw} = K_{Pw} \cdot \gamma_p$ (6.a)

Transverse flanges $Q_{POF} = K_{POF} \cdot \gamma_p$ (6.b)

Concrete of core and its side $Q_{PCO} = K_{PCO} \cdot \gamma_p$ (6.c)

Cover concrete $Q_{PCOV} = K_{PCOV} \cdot \gamma_p$ (6.d)

in which

$$K_{Pw} = E_{SW} \cdot c_h \cdot c_{t_w} / 2.6,$$

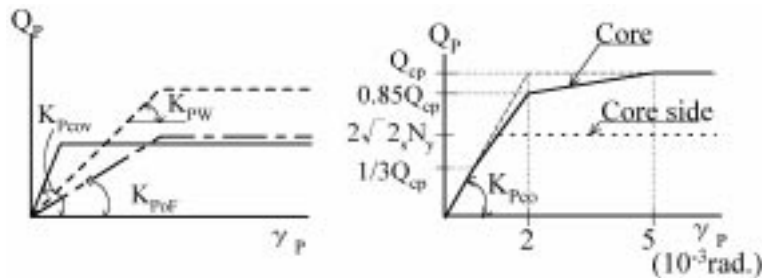


Fig. 14 Assumed $Q_p - \gamma_p$ relationships

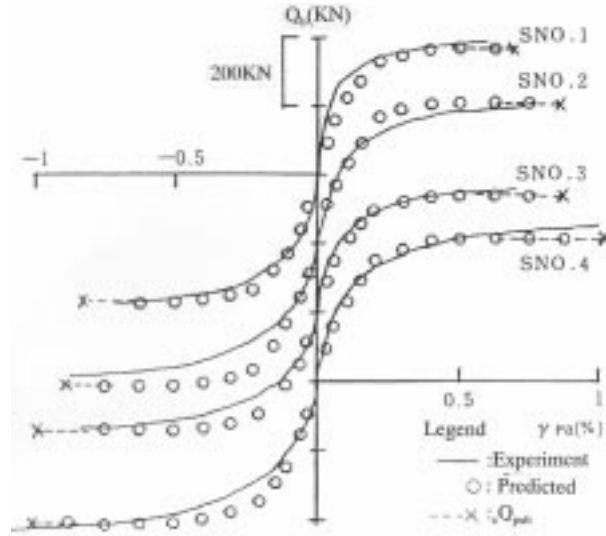


Fig. 15 Synthetic curves of Q_b - γ_{pa} relationships

$$K_{POF} = 2E_{sf} \cdot b \cdot h \cdot c_f / [\{2.6\kappa + (b h_w / c_f)^2\} b h_w],$$

$$K_{PCO} = E_c \cdot c h_w \cdot b h^3 \cdot c h^2 / \{4(b h^2 + c h^2 / 4)^2\},$$

$$K_{PCOV} = E_c \cdot c D - c h \cdot c j / 2.4,$$

where E_{sw} , E_{sf} : Young's modulus of steel, E_c : Young's modulus of concrete, κ : Shape factor (1.2), where assumed elastic Poisson ratios were respectively 0.3 for steel and 0.2 for concrete.

Also, as shown in Fig. 14, the Q_p - γ_p relationships of each part were assumed as follows. Firstly, in the column web, the column crossing flange and the covering concrete part, perfectly elasto-plastic models were adopted. Secondly, in the concrete core part and the concrete core side part, Q_{PCO} - γ_p relationships including compression characteristics of concrete were adopted.

The comparison between the predicted curves ($Q_b(=Q_p/(2l_b/bh - L/H)) - \gamma_p$) and the measured synthetic curves of beam load (Q_b)-shear distortion (γ_{pa}) are shown in Fig. 15. From the figure, it is observed that the predicted curves are in fairly high agreement with the measured synthetic curve.

5. Conclusions

The conclusions attained are as follows:

(1) SRC subassemblages with the proposed beam-column joints show adequate seismic performances which is superior to the demand of the current code.

(2) The yield and ultimate strength capacities of the beam-to-column connections can be estimated by analysis based on the yield line theory.

(3) The skeleton curves and the ultimate shear capacities of the beam-column joint panel are fairly well predicted by considering the simple stress transfer mechanism.

References

- Architectural Institute of Japan (1987), "Standard for structural calculation of steel reinforced concrete structures", (in Japanese).
- Architectural Institute of Japan (1990), "Ultimate strength and deformation capacity of buildings in seismic design (1990)", (in Japanese).
- Federal Emergency Management Agency (2000), "FEMA-350 recommended seismic design criteria for new steel moment-frame buildings".
- Kato, B. (1982), "Beam-to-column connection research in japan", *Journal of Structural Division*, ASCE, **108**(ST2), 343-360.
- Matsui, K., Tsuda, K. and Nakatsuji, H. (1989), "Studies for development on rational design of arrangement of reinforcing bars in SRC structure", *Summarizes of Technical Papers of Annual Meeting, Architectural Institute of Japan*, 1563-1564 (in Japanese).
- Morita, K., Yokoyama, Y., Hiraoka, H. and Ishii, T. (1990), "Structural behaviors of steel-beam to SRC-column Connections reinforced with vertical stiffening plates", *Journal of Structural and Construction Engineering (Transaction of AIJ)* No. 413, 53-64 (in Japanese).
- Taniguchi, K., Fujiwara, S., Tanioka, T., Nishimura, T. and Minami, K. (1988), "Transverse reinforcing bar details in composite beam-column joints", *Summarizes of Technical Papers of Annual Meeting, Architectural Institute of Japan*, 1305-1308 (in Japanese).
- Teraoka, M., Morita, K., Fujiwara, K. and Sasaki, S. (1992), "Experimental study on simplified SRC beam-to-column joints in construction technology", *Summarizes of Technical Papers of Annual Meeting, Architectural Institute of Japan*, 1755-1758 (in Japanese).
- Teraoka, M., Morita, K. and Sasaki, S. (2000), "Experimental study on simplified SRC beam-column joints in construction technology", COMPOSITE AND HIBRID TECHNOLOGY, Proceedings of 6th ASCCS Conference, 773~744, Los Angeles, USA.
- Umemura, H. (1951), "Plastic deformation and ultimate strength on reinforced concrete beam", *Transaction of The Architectural Institute of Japan* No. 42, 59-70 (in Japanese).
- CC